

PReD: An LLM-based Foundation Multimodal Model for Electromagnetic Perception, Recognition, and Decision

Zehua Han Jing Xiao Yiqi Duan Mengyu Xiang Yuheng Ji
 Xiaolong Zheng Chenghanyu Zhang Zhendong She Junyu Shen Dingwei Tan
 Shichu Sun Zhou Cong Mingxuan Liu Fengxiang Wang Jinping Sun
 Yangang Sun

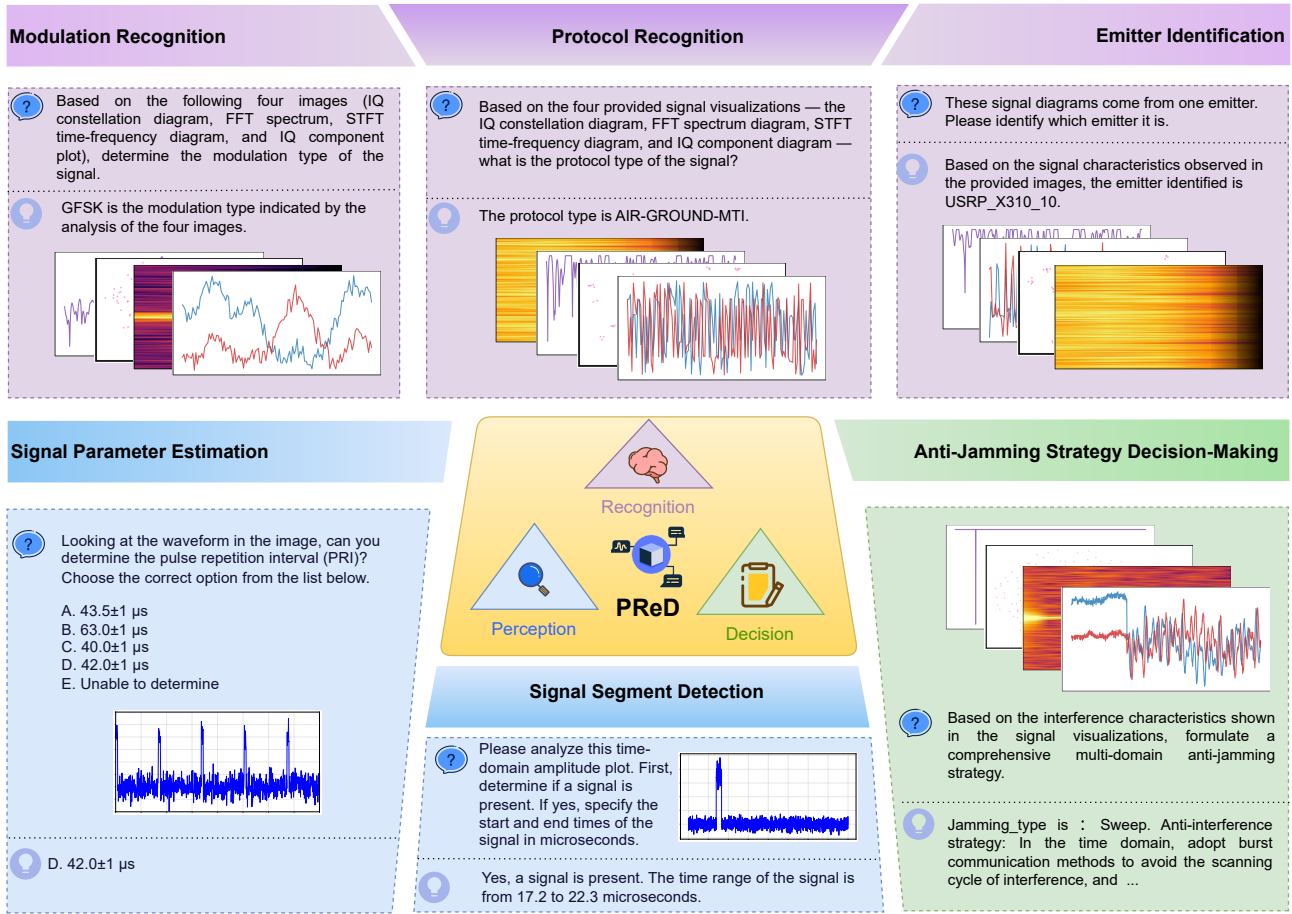


Figure 1. Overview of PReD and its capabilities, instantiated across six core electromagnetic (EM) tasks that span the three tiers of perception, recognition, and decision-making. The figure demonstrates how PReD processes multi-view signal visualizations to address a diverse range of EM instructions, from quantitative parameter estimation to open-ended anti-jamming strategy generation.

Abstract

Multimodal Large Language Models have demon-

strated powerful cross-modal understanding and reasoning capabilities in general domains. However, in the electromagnetic (EM) domain, they still face chal-

allenges such as data scarcity and insufficient integration of domain knowledge. This paper proposes *PReD*, the first foundation model for the EM domain that covers the intelligent closed-loop of "perception, recognition, decision-making." We constructed a high-quality multitask EM dataset, *PReD-1.3M*, and an evaluation benchmark, *PReD-Bench*. The dataset encompasses multi-perspective representations such as raw time-domain waveform, frequency-domain spectrograms, and constellation diagrams, covering typical features of communication and radar signals. It supports a range of core tasks, including signal detection, modulation recognition, parameter estimation, protocol recognition, radio frequency fingerprint recognition, and anti-jamming decision-making. *PReD* adopts a multi-stage training strategy that unifies multiple tasks for EM signals. It achieves closed-loop optimization from end-to-end signal understanding to language-driven reasoning and decision-making, significantly enhancing EM domain expertise while maintaining general multimodal capabilities. Experimental results show that *PReD* achieves state-of-the-art performance on *PReD-Bench* constructed from both open-source and self-collected signal datasets. These results collectively validate the feasibility and potential of vision-aligned foundation models in advancing the understanding and reasoning of EM signals.

1. Introduction

Recent multimodal large language models (MLLMs), enabled by instruction tuning and cross-modal alignment, have achieved notable breakthroughs on visual question answering, retrieval, and reasoning tasks (e.g., LLaVA [1], BLIP-2 [2], GPT-4V [3], ImageBind [4]), driving a unified intelligence paradigm that uses natural language as the primary interface. However, these general-purpose large language models (LLMs) principally rely on world knowledge and language-reasoning capabilities derived from image, video, and audio modalities; they lack intrinsic representations of electromagnetic (EM) signal priors such as raw In-phase and quadrature (I/Q) waveforms, spectrogram structures, constellation geometry, micro-Doppler signatures, and cyclostationarity. This deficit limits their applicability in high-demand domains such as spectrum management, wireless security, and radar semantic understanding, where expert-level, auditable reasoning about EM signals is required. Meanwhile, EM-/wireless-oriented LLM efforts have emerged (e.g., WirelessLLM [5], RadioLLM [6], RFF-LLM [7]), but many of these concentrate on network planning [8, 9] or knowledge-level QA [10] and treat signal features as

external prompts rather than forming a unified foundation for raw EM data. Together, these observations indicate that an integrated "model–data–evaluation" framework tailored to the shapes and task ecology of EM data is essential.

A primary challenge in the EM domain is constructing datasets suitable as inputs to large EM models. Public EM signal repositories are scarce or insufficient: many are generated from simulations or cover single communication scenarios, with limited diversity in modulation formats, protocol stacks, and interference types [11]. Representative datasets such as RadioML2016 [12], RadioML2018 [13], and Hisar-Mod2019.1 [14] are widely used in research but are not directly fit for training and evaluating EM large models. Second, unified multi-task capability is lacking: tasks including signal detection, modulation recognition, parameter estimation, protocol classification, radio frequency (RF) fingerprinting, and anti-jamming strategy selection are typically modeled separately, and there is no widely adopted base that unifies these tasks in a shared multimodal EM feature space aligned with instruction-driven interfaces. Third, a clear expert gap exists when transferring general-purpose MLLMs to the EM domain: a general-purpose LLMs often fails to internalize EM priors (e.g., cyclostationarity, carrier/symbol timing, inter-band coupling), yielding unstable perception and reasoning under low SNR, strong interference, or complex waveforms, and limiting interpretability.

Existing EM large-model research typically focuses on single-task or knowledge-centric intelligence. For example, WirelessLLM emphasizes knowledge alignment, rule understanding, and network optimization but rarely operates directly on raw I/Q waveforms or spectrograms [5]. RadioLLM integrates LLMs in cognitive radio via prompt and token reprogramming [6], yet it remains largely a "languagefeature prompt" approach and doesn't deliver an end-to-end perceptual-to-decisional capability from signals to semantic actions. In classical RF machine learning, deep models have advanced modulation classification, time-frequency feature modeling, synchronization/registration, and protocol-sequence recognition, but these successes are typically confined to task-specific, small-scale models with limited data and lack instruction alignment and standardized evaluation that would support closed-loop perception, recognition, and decision-making generalization and verifiability [15–17].

We present a unified foundation model for EM perception, recognition, and decision-making, termed **PReD**. An overview of our entire framework is provided in Fig 1. At the data layer, we construct multi-

dimensional, feature-visualized signal corpora that raw I/Q waveform, frequency-domain spectrum, short-time Fourier transform (STFT) spectrograms, and constellation diagrams. Eight human annotators provide reasoning-style descriptions and consistency labels under a unified question-answer protocol, forming multi-granularity supervision for multiple task families, including signal segment detection (SSD), signal parameter estimation (SPE), modulation recognition (MR), protocol recognition (PR), emitter identification (EI), and anti-jamming strategy decision-making (AJSD). At the model layer, we design a visual input paradigm that jointly represents EM signals from complementary views across time, frequency, and constellation domains, and adopt a multi-stage training pipeline to support multi-task learning at scale. At the learning paradigm level, we introduce unified multi-task instruction alignment that uses language as a cross-task interface, enabling an end-to-end loop from perception to recognition and to decision-making. This design retains the cross-modal expressiveness of general multimodal large language models while compensating for missing EM priors.

The main contributions are as follows:

- To the best of our knowledge, this work proposes and implements the first integrated foundation model for the EM domain that unifies perception, recognition, and decision-making.
- To support efficient training and comprehensive evaluation, we build a large-scale, cross-view EM dataset that covers time, frequency, time-frequency, and constellation perspectives with reasoning-style supervision.
- Extensive experiments indicate competitive performance across diverse EM tasks; datasets, models, and related code will be released to facilitate further research.

2. Related Work

Recent years have seen sustained advances in Large Language Models (LLMs) and multimodal variants (MLLMs) [18]. Via instruction tuning, cross-modal alignment, and tool augmentation, these systems advance general-purpose intelligence in visual question answering, retrieval, reasoning, and open-world understanding [19]. Representative image-text models include BLIP-2 [2], LLaVA [1], MiniGPT-4 [20], and Qwen-VL [21]; unified cross-sensor representations are explored by ImageBind [4]; long-context video-text and tool integration are addressed by Flamingo [22], Kosmos-2 [23], and GPT-4Vis [24]. Together, these works construct transferable interfaces among natural images, audio and speech, web corpora, and lan-

guage patterns, enabling a language-centered multitask paradigm [25].

2.1. General-Purpose Multimodal Large Models

A prevailing design treats an LLM as the semantic hub coupled with vision and audio encoders. Cross-modal alignment is realized through projection heads or query routers, and instruction tuning with preference optimization harmonizes multitask behavior. This “backbone-alignment-instruction” pipeline has become a standard for reasoning over images, video, and speech [26]. *Transfer to EM is nontrivial*: (i) missing modality priors cyclostationarity, carrier/symbol timing offsets, phase envelope and constellation geometry, inter-band spectral coupling, and micro-Doppler are not captured by features from natural image or audio corpora [27, 28]; (ii) interface mismatch beyond categorical recognition, EM requires regression and closed-loop control (e.g., SNR and timing-offset estimation, channel/jammer recovery, synchronization, anti-jamming search), whereas generic instruction spaces emphasize QA-style generation [29]; (iii) supervision/metric mismatch datasets seldom provide executable physical ground truths or counterfactual controls, encouraging semantic plausibility over testable EM correctness.

2.2. Large-Model Directions in the EM Domain

Knowledge alignment and cognitive-radio-oriented work. WirelessLLM targets network planning, rule understanding, and knowledge-based QA for cognitive wireless decisions but seldom operates directly on raw I/Q waveforms or spectrograms [5]. RadioLLM introduces prompt and token reprogramming to embed LLMs in cognitive-radio workflows and improves programmability, yet it remains a language-external-feature paradigm without unified modeling of raw EM data [6]. RFF-LLM enhances device-level interpretability via language interfaces but is limited by single-task scope and controlled data [7]. *Synthesis of limitations*: existing approaches rarely cover, within one framework, signal detection, modulation/protocol recognition, emitter identification, parameter estimation, and anti-jamming decision-making under a unified instruction space; moreover, EM-derived features are often used as auxiliary prompts rather than a joint representation enforcing cross-view consistency among I/Q, spectrum, spectrograms, and constellations, which weakens robustness in low-SNR regimes. These gaps motivate EM-tailored foundation models that integrate data, modeling, and evaluation to close the loop across perception, recognition, and decision-making for auditable EM intelligence [30].

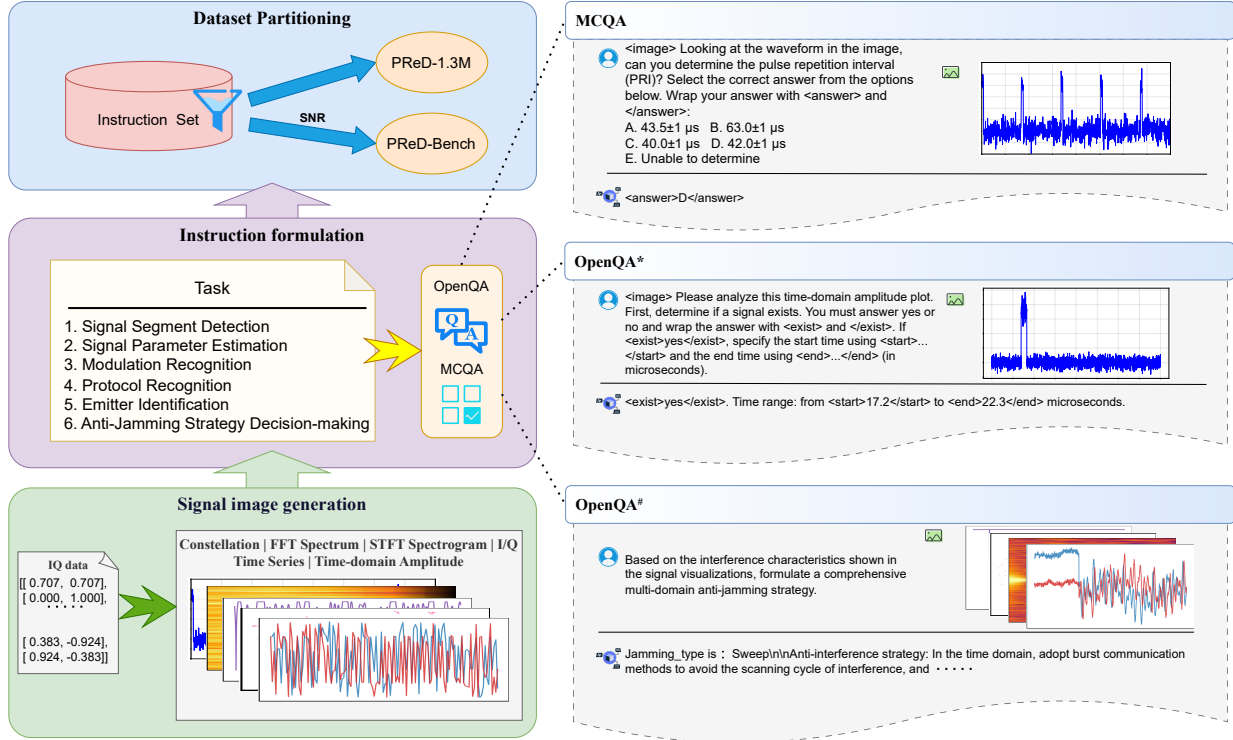


Figure 2. Overall pipeline for the construction of the PReD-1.3M training set and the PReD-Bench. We first generate five types of signal visualizations from the raw IQ signals. We then create corresponding OpenQA and MCQA pairs for each task type to form a complete instruction set. Finally, a portion of this set is sampled to obtain the PReD-Bench, which is kept strictly separate from the training data.

3. The PReD Dataset and Benchmark

In this section, we detail the construction of our large-scale EM instruction corpus, PReD-1.3M, and our hierarchical evaluation benchmark, PReD-Bench. Figure 2 illustrates the overall pipeline, which begins with signal visualization, proceeds to instruction formulation, and concludes with the partitioning of the instruction set into training and evaluation splits. We begin by describing the shared methodology for data formulation.

3.1. Signal Representation and Task Formulation

The EM instruction formulation defines six core tasks: SSD, SPE, MR, PR, EI, and AJSD. Each instruction is paired with visual signal representations such as waveform, FFT spectrum, STFT spectrogram, or constellation images. Multi-format question-answer templates (OpenQA and MCQA) are used to synthesize benchmark-ready supervision for MLLMs training.

An EM signal is fundamentally a complex-valued time series $x[n] \in \mathbb{C}^N$. We map each raw sample to four complementary visual views:

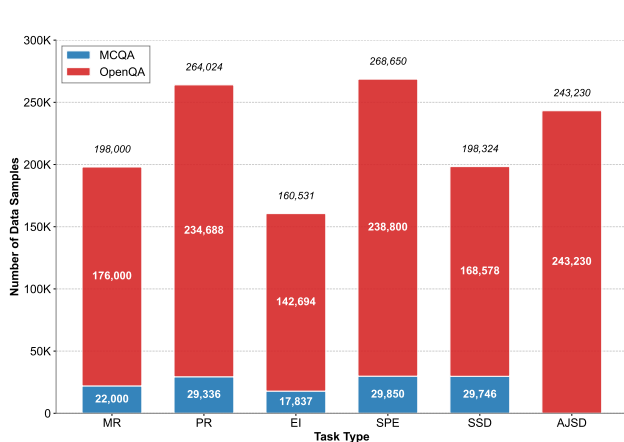
- **I/Q Constellation** sampled scatter points $\{x[k]\}$ that reveal symbol constellations and modulation

geometry;

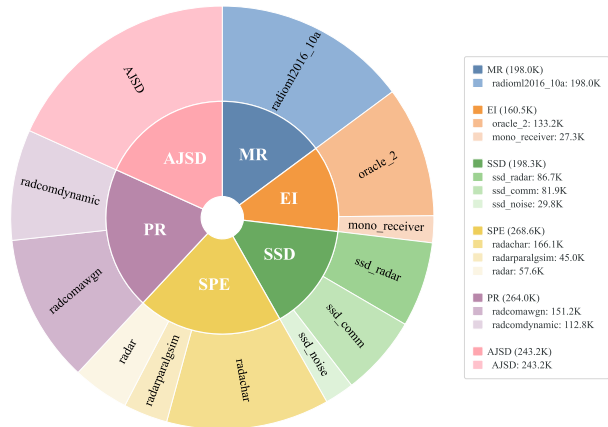
- **FFT Magnitude Spectrum** $S_{\text{FFT}}(f) = |\text{FFT}(x[n])|$, capturing bandwidth and frequency-domain structure;
- **STFT Spectrogram** $S_{\text{STFT}}(t, f)$, trading off timefrequency resolution to reveal pulsed or sweep patterns;
- **Raw I/Q Waveform** real and imaginary component trajectories $x_I[n]$ and $x_Q[n]$, together with the amplitude envelope for parameter readout.

To support instruction-style training [31], we design two question formats and corresponding output tags. Each signal sample in MCQA format includes a built-in "Unable to answer" option to mitigate model overconfidence on ambiguous inputs.

- **Multiple Choice Question-Answer Pairs:** the user presents four images and five options (including **Unable to answer**); the assistant returns `<answer>A</answer>` [32].
- **Open-ended Question-Answer Pairs:** the user provides four images and instructs "to only output the result"; the assistant responds with a structured tag such as `<mode></mode>`, facilitating auto-



(a) Task-wise sample counts split by OpenQA (red) and MCQA (blue).



(b) Source composition per task (outer ring) organized by six top-level tasks (inner ring).

Figure 3. Scale and composition of the EM training dataset across six tasks and two QA formats.

mated scoring and downstream integration [33].

3.2. The PReD-1.3M Corpus

To facilitate the domain adaptation of our model, we construct **PReD-1.3M**, a large-scale EM instruction corpus. As summarized by the task-wise histogram in Fig. 3a, the corpus totals 1.33×10^6 question-answer pairs. OpenQA supervision constitutes the majority (approximately **90.3%**), with the remaining $\sim 9.7\%$ provided in the MCQA format. The sunburst chart in Fig. 3b details the source composition for each task, demonstrating a rich mix of public and controllable synthetic corpora. The corpus is broken down by task as follows:

(A) Signal Segment Detection. We aggregate three sources `radar`, `communication`, and `noise` to form a supervised corpus of short complex-baseband (IQ) segments acquired at 20 MS/s with SNR spanning $[-10, 20]$ dB. The noise-only subset is retained as hard negatives. The dataset comprises $\approx 1.98 \times 10^5$ labeled segments.

(B) Signal Parameter Estimation. The parameter estimation task is cast into an instruction format that requests quantities such as pulse width, period, count, and time delay. The input is a single time-domain amplitude trace, and the correct MCQA choice is provided as value $\pm 1 \mu\text{s}$. Distractors are generated using multiplicative, offset, and random-sampling strategies, and options that are too close to the ground truth are removed to increase separability. The parameter-estimation set contains 269K samples

(OpenQA: 239K; MCQA: 30K), spanning multiple f_s settings (e.g., 10/12 MHz) and approximately covering $[-20, +20]$ dB in SNR.

(C) Modulation Recognition. The modulation recognition task is built on RadioML2016.10a. We fix $f_s = 1$ MHz and sample SNR uniformly over $[-20, +18]$ dB. Modulation classes include AM-DSB/SSB, BPSK/QPSK/8PSK, QAM16/64, GFSK, CPFSK, PAM4, WBFM, etc. Each sample is rendered into four images, and two instruction types (OpenQA and MCQA) are generated. The modulation dataset totals 198K samples (OpenQA: 176K; MCQA: 22K).

(D) Protocol Recognition. The protocol dataset covers avionics ranging, surveying, beacons, short-range protocols, Bluetooth, IEEE 802.11 / 802.15.4, and other protocols. The typical sampling rate is $f_s = 10$ MHz. Examples are generated via instruction-style QA. The constructed protocol dataset contains 263K samples (OpenQA: 234K; MCQA: 29K). SNRs are sampled within $[-20, 18]$ dB.

(E) Emitter Identification. For emitter identification, we collect real and simulated receiver-chain variations to create device fingerprints (Oracle_2 / Mono-Receiver basis). Device names are prefixed in the templates (e.g., USRP B210/X310 N), and `Unable_to_answer` is retained to filter ambiguous boundary cases. The EI dataset comprises 161K samples (OpenQA: 143K; MCQA: 18K), covering multiple sampling rates and a long-tailed device distribution.

Dimension	Task	OpenQA	MCQA
EM Perception	SPE	2250	750
	SSD	1700	300
	MR	–	500
EM Recognition	PR	–	500
	EI	–	458
EM Decision-making	AJSD	2000	–

Table 1. PReD-Bench for perception, recognition, and decision-making. Abbreviations: SSD = Signal Segment Detection; SPE = Signal Parameter Estimation; MR = Modulation Recognition; PR = Protocol Recognition; EI = Emitter Identification; AJSD = Anti-Jamming Strategy Decision-making. OpenQA and MCQA denote open-ended and multiple-choice question-answer pairs, respectively.

(F) Anti-Jamming Strategy Decision-Making.

We include pure-noise examples, single- and multiple-interferer regimes, linear frequency modulation, phase-coded waveforms, and diverse radar modes. We provide causal OpenQA pairs for AJSD task to strengthen the model’s strategy decision-making capability.

3.3. The PReD-Bench Benchmark

To systematically evaluate general-purpose models in the EM domain, we introduce a hierarchical EM domain benchmark. The benchmark is constructed via SNR-stratified sampling and is kept strictly isolated from the PReD-1.3M training set to prevent any data leakage. It organizes the perception-recognition-decision-making pipeline into six representative tasks, with unified I/O conventions and scoring for both OpenQA and MCQA. Table 1 specifies the exact per-task item counts by question type. Data are curated from multi-origin public sets and controllable simulation, followed by normalization and quality auditing. Prompts and rubric-based scoring are standardized to enable cross-task comparability and reproducible evaluation, and anti-jamming strategy decision-making is explicitly included to stress closed-loop reasoning under adversarial EM conditions [34].

4. PReD Model

4.1. Model Architecture

PReD adopts a standard yet effective multimodal architecture inspired by LLaVA [35], comprising three key components: a vision encoder, a projector, and a large language model decoder.

Core Components. We employ SigLIP as the vision encoder (f_v) to extract features from each visual view (X_k). A two-layer MLP projector (g) then maps these visual tokens into the embedding space of the lan-

guage model. For the decoder, we utilize the pretrained Qwen3-8B [36] model (ϕ).

Multi-View and Text Integration. To handle multiple views, we follow a standard packing strategy where visual tokens from each view are concatenated, separated by a learnable boundary token, and augmented with a view-index embedding [37]. This packed visual prefix, denoted as $\Pi(\mathcal{X})$, is then prepended to the tokenized instruction prompt P . The entire sequence is processed by the single autoregressive Qwen3-8B decoder, which models the probability of the response sequence Y as shown in Eq. (1). Our training methodology, which involves progressively unfreezing and fine-tuning these components, is detailed in Section 4.2.

$$p_\phi(Y | C) = \prod_{t=1}^L p_\phi(y_t | C, y_{<t}), \quad (1)$$

Training Objective. We define the language modeling loss

$$\mathcal{L}_{\text{LM}}(\phi) = - \sum_{t=1}^L \log p_\phi(y_t | C, y_{<t}). \quad (2)$$

4.2. Multi-Stage Training

To couple general multimodal competence with EM expertise, we train PReD with a four-stage curriculum.

Stage-1: Projector Warm-Up. We freeze ϕ_0 , f_v and train g on single-view inputs to align vision tokens at a 384 resolution and 729 vision-token length.

Stage-2: General Single-View. We unfreeze the full model and train with general single-image corpora, using up to 5×729 tokens to consolidate instruction following.

Stage-3: General Multi-View. We introduce multi-view inputs (up to 10×729 tokens) to develop cross-view reasoning. To preserve single-view competence, we adopt the LLaVA-Next interleaving strategy, mixing the new data with 40% of the Stage-2 corpus.

Stage-4: EM Domain Adaptation. Finally, for domain adaptation, the model is fine-tuned on our PReD-1.3M dataset, covering all six EM tasks. To retain generalist skills, we continue this interleaving approach by mixing the specialized data with 25% of the Stage-2 single-view and 50% of the Stage-3 multi-view corpora. Training schedules follow Table 2.

5. Experiment and Results

5.1. Performance Evaluation of EM Tasks

Table 3 demonstrates that across the perception-recognition-decision-making pipeline, PReD

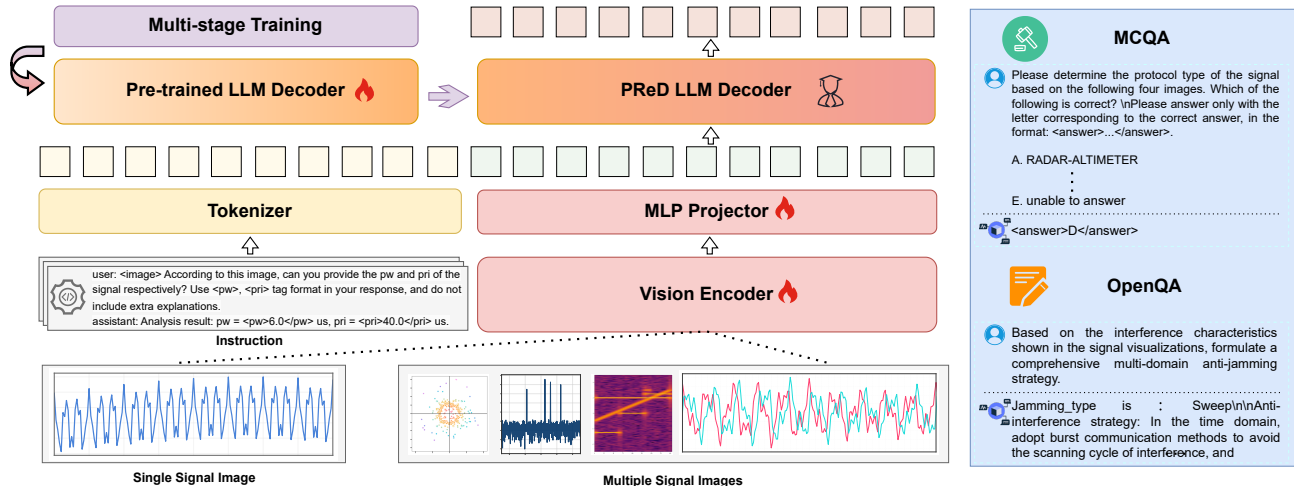


Figure 4. Overall pipeline of PReD. (Bottom to top) Multi-view EM renderings are encoded and projected into the token space, where they are combined with tokenized instructions. A pre-trained LLM decoder is first aligned with visual features and then fine-tuned through a multi-stage curriculum to become the specialized *PReD LLM Decoder*. The model supports two output modes: open-ended generation (OpenQA) and structured multiple-choice question answering (MCQA).

Category	Hyperparameter	Stage-1	Stage-2	Stage-3	Stage-4
Vision	Resolution	384	Max 384 × (2 × 2)	Max 384 × (6 × 6)	Max 384 × (6 × 6)
	Tokens	729	Max 729 × 5	Max 729 × 10	Max 729 × 10
Data	Dataset	LCS	General Single-Image	General Multi-Image*	PReD-1.3M*
	Samples	558K	858K	832K	1.8M
Model	Trainable Components	Projector	Full Model	Full Model	Full Model
	Tunable Parameters	21.5M	8.6B	8.6B	8.6B
Training	Per-Device Batch Size	8	4	2	2
	LR: ψ_{ViT}	N/A	2×10^{-6}	2×10^{-6}	2×10^{-6}
	LR: $\{\theta_{Proj}, \phi_{LLM}, \phi_{LoRA}\}$	1×10^{-3}	1×10^{-5}	1×10^{-5}	1×10^{-5}
	Epochs	1	1	1	1

Table 2. Training schedule for PReD across four stages on 16 NVIDIA A100 GPUs (80GB each). A star * indicates datasets mixed with general visual corpora from earlier stages.

consistently outperforms all general-purpose baselines and remains strong in the decision-making stage that requires untagged, generative matching (OpenQA). The results reveal a clear capability boundary: while general-purpose models show rudimentary skill on simple perception tasks for instance, GPT-5 achieves 61.0 accuracy on the SSD (MCQA) task they completely fail at complex recognition and decision-making. This is most evident in the anti-jamming (AJSD) task, where all generalist models score near zero on BLEU4, proving incapable of generating valid strategies. In contrast, PReD excels (BLEU4=0.253).

This confirms that generalist models are limited to shallow pattern matching due to a lack of domain priors, whereas PReD successfully forges the full perception-to-decision pipeline via its specialized architecture.

5.2. Evaluation on General Multimodal Benchmarks

An important question is whether PReDs domain-oriented optimization affects its general multimodal understanding capabilities. To investigate this, we conducted comprehensive evaluations on several widely

Model	EM Perception				EM Recognition			EM Decision-Making			
	SSD		SPE		MR	PR	EI	AJSD (OpenQA#)			
	MCQA	OpenQA*	MCQA	OpenQA*	MCQA	MCQA	MCQA	BLEU4	ROUGE	METEOR	CIDEr
qwen2.5-vl-7b [†] [38]	28.7	0.2	20.5	0.1	24.2	14.0	–	0.000	0.079	0.115	0.128
qwen3-vl-8b [†] [36]	21.3	1.3	18.8	2.0	11.6	2.8	–	0.000	0.094	0.121	0.228
qwen3-vl-235b-a22b [†] [36]	27.7	0.5	30.4	2.0	20.2	8.6	–	0.000	0.090	0.070	0.151
seed-1.6 vision [39]	41.3	1.5	40.4	3.1	23.4	21.4	–	0.000	0.095	0.039	0.169
claude sonnet-4 [40]	28.7	1.4	48.5	2.8	25.2	21.6	–	0.000	0.103	0.078	0.154
GPT-5 [41]	61.0	7.2	42.9	13.3	12.0	19.2	–	0.000	0.017	0.028	0.055
gemini-2.5 pro [42]	25.3	6.2	56.3	12.0	29.0	24.0	–	0.000	0.081	0.036	0.129
PReD (Ours)	99.3	80.6	97.1	81.9	72.0	72.0	69.4	0.253	0.559	0.515	0.617

Table 3. Benchmark results for EM perception, recognition, and decision-making tasks. A superscript [†] marks an Instruct (instruction-tuned) variant. **OpenQA*** indicates answers with a specific tag whose results are directly matched; **OpenQA#** indicates answers without a specific tag, where matching is performed using BLEU4, ROUGE, METEOR, and CIDEr. Since EI task requires device-specific RF fingerprint learning, general MLLMs are not comparable and their results are omitted.

Model	MMStar	AI2D	HallusionBench	SEEDBench IMG	POPE	ScienceQA TEST	Average
GPT-4v [3]	49.7	75.9	46.5	71.6	75.4	82.1	66.9
PReD (Ours)	50.2	74.3	54.5	73.7	70.4	69.2	65.4
Qwen-VL-Max [43]	49.5	75.7	41.2	72.7	71.9	80.0	65.2
LLaVA-Next-Interleave-7B [44]	44.5	73.8	34.8	72.0	85.5	73.2	64.0
DeepSeek-VL-7B [45]	40.5	65.3	34.5	70.1	85.6	80.9	62.8
MiniCPM-V-2 [46]	39.1	62.9	36.1	67.1	86.3	80.7	62.0
ShareGPT4V-7B [47]	35.7	58.0	28.6	69.3	86.6	69.5	58.0

Table 4. Results on general multimodal benchmarks.

used benchmarks (see Table 4). Our main comparisons include representative open-source models of similar scale, with LLaVA-Next-Interleave-7B serving as a key methodological reference.

The results show that PReD achieves an average score of 65.4, slightly surpassing its reference model LLaVA-Next (64.0) and on par with other strong open-source baselines such as Qwen-VL-Max (65.2). This indicates that PReD successfully maintains competitive general multimodal understanding while benefiting from its domain-oriented enhancements.

For a broader perspective, we also report results from the high-performance proprietary reference GPT-4V (1106-preview, Nov. 2023). PReD demonstrates comparable overall capability (65.4 vs. 66.9) and notably achieves stronger robustness on HallusionBench (54.5 vs. 46.5). This suggests that our proposed training paradigm may contribute to improved reliability under hallucination-prone scenarios. In summary, PReD illustrates the potential of building a foundation model that effectively integrates domain expertise with broad generalization ability.

6. Conclusions

We have presented **PReD**, the first foundation model to unify the full pipeline of perception, recognition, and decision-making in the EM domain. Our core methodology involves a novel, large-scale EM corpus, PReD-1.3M, which represents signals via complementary visual views, coupled with a multi-stage curriculum to progressively instill domain expertise. Extensive experimental validations demonstrate that PReD significantly outperforms current state-of-the-art general-purpose MLLMs on PReD-Bench, a benchmark specifically tailored for evaluating EM intelligence. This substantiates PReD’s superior specialized proficiency within this particular scientific domain. Crucially, PReD achieves this specialized excellence while maintaining strong, competitive performance on standard multimodal benchmarks, demonstrating that domain specialization need not come at the cost of general vision-language capabilities. Our work not only charts a scalable path for EM intelligence but also validates the immense potential of adapting vision-aligned foundation models to other complex scientific domains.

Appendix

This appendix provides supplementary material that delves into the architectural details, training methodology, evaluation protocols, and extensive experimental analysis of the PReD model. We begin by detailing the four-stage curriculum training pipeline for PReD (Sec. A), covering data composition, progressive tuning strategies, and key hyperparameters. This is followed by a description of the automatic metrics used to assess free-form answers in our `OpenQA#` setting (Sec. B). Subsequently, we present a series of complementary experiments (Sec. C) designed to offer deeper insights, including a critical ablation study on the domain-specific expertise stage to demonstrate the prevention of catastrophic forgetting, a systematic analysis of input modality contributions, an out-of-domain generalization test, and a robustness analysis across varying Signal-to-Noise Ratios (SNR). Finally, to provide a more intuitive understanding of our work, we include additional visual and qualitative analyses (Sec. D and beyond), featuring a hierarchical visualization of the PReD-Bench composition, a comparative radar plot of model performance, and representative case studies showcasing PReD’s capabilities across the full spectrum of EM tasks.

A. Details of Training Pipeline for PReD

PReD is built on Qwen-3 and a pre-trained SigLIP vision encoder, and is trained with a four-stage curriculum. Fig. 5 provides an overview of the data composition across stages, while Table 5 summarizes the corresponding hyperparameters and training schedule.

The curriculum begins with **Stage 1 (Pretrain)**, a warm-up phase that exclusively trains the **projector** using a relatively high learning rate of 1×10^{-3} , while both the **vision encoder (ViT)** and the **language model** remain frozen. This stage utilizes the `blip_laion_cc_sbu_558k` dataset to establish initial **vision–language alignment**. As shown in Table 5, it operates with a base resolution of 384, a token budget of 729, and a *flat* patch merging strategy.

From **Stage 2** onward, the full model is progressively unfrozen for **end-to-end tuning**. In **Stage 2** (26.5%; 858,231 samples), we introduce data from `LLaVA-UHD-v2-SFT-Data` to consolidate single-image instruction-following capabilities. A **decoupled learning-rate scheme** is applied: the ViT branch is fine-tuned with 2×10^{-6} , while the projector and language-model parameters are updated with 1×10^{-5} . Correspondingly, the spatial coverage is expanded to $\text{Max } 384 \times (2 \times 2)$ and the visual token budget is increased to $\text{Max } 729 \times 5$. The **patch merging strat-**

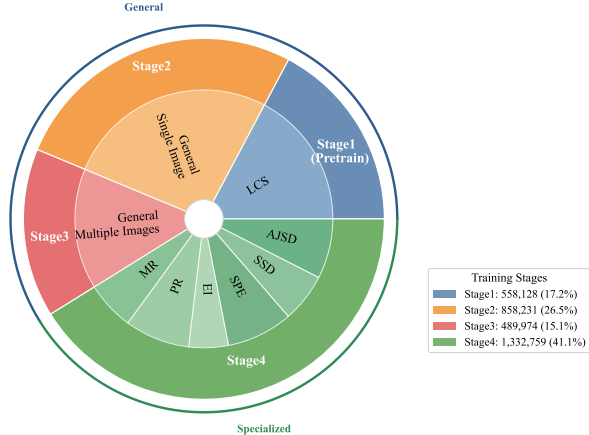


Figure 5. Overview of our four-stage curriculum and data composition. The outer ring shows the training stages; the middle ring indicates data regimes (LCS, general single/multi-image); the inner ring lists EM tasks (SSD, SSE, MR, PR, EI, AJSD) emphasized in Stage 4. Percentages denote the proportion of samples used per stage.

egy is switched to `spatial_unpad` in this stage to better handle the gridded visual inputs.

Stage 3 (15.1%; 489,974 samples) incorporates multi-image data from the `M4-Instruct-Data` dataset to enable **multi-view modeling**. To balance computational cost and efficiency, we filter out 3D and video samples from this dataset, resulting in a final subset of 489,974 samples that focuses on static multi-view inputs. **To retain previously learned capabilities, the training set for this stage is mixed with 40% of the general single-image corpus from Stage 2.** This stage marks a significant expansion of model capacity: the spatial coverage and token budget are further increased to their maximums of $\text{Max } 384 \times (6 \times 6)$ and $\text{Max } 729 \times 10$. To accommodate the longer context, the maximum sequence length is also doubled from 4,096 to 8,192.

Stage 4 (41.1%; 1,332,759 samples) focuses on fine-tuning the model for **specialized EM tasks** using our curated `PReD-1.3M` dataset. This final stage maintains the maximal spatial coverage and token capacity established in Stage 3. **Furthermore, to prevent catastrophic forgetting of general abilities, the training corpus is augmented by mixing in 25% of the Stage 2 single-image corpus and 50% of the Stage 3 multi-image corpus.**

Across all four stages, optimization uses AdamW with DeepSpeed-Zero3, a cosine learning-rate schedule, weight decay of 0, and a warmup ratio of 0.03. The projector employs an `mlp2x2_gelu` head, and the

Category	Hyperparameter	Stage-1	Stage-2	Stage-3	Stage-4
Vision	Resolution	384	Max $384 \times (2 \times 2)$	Max $384 \times (6 \times 6)$	Max $384 \times (6 \times 6)$
	Tokens	729	Max 729×5	Max 729×10	Max 729×10
Model	Trainable Components	Projector	Full Model	Full Model	Full Model
	Tunable Parameters	21.5M	8.6B	8.6B	8.6B
Training	Per-device Batch Size	8	4	2	2
	Gradient Accumulation	1	1	1	1
	LR: ψ_{ViT}	N/A	2×10^{-6}	2×10^{-6}	2×10^{-6}
	LR: $\{\theta_{\text{Proj}}, \phi_{\text{LLM}}\}$	1×10^{-3}	1×10^{-5}	1×10^{-5}	1×10^{-5}
	Epoch	1	1	1	1
	Optimizer	AdamW	AdamW	AdamW	AdamW
	Deepspeed	Zero3	Zero3	Zero3	Zero3
	Weight Decay	0	0	0	0
	Warmup Ratio	0.03	0.03	0.03	0.03
	LR Schedule	cosine	cosine	cosine	cosine
	Projector Type	mlp2x2_gelu	mlp2x2_gelu	mlp2x2_gelu	mlp2x2_gelu
	Vision Select Layer	-2	-2	-2	-2
	Patch Merge Type	flat	spatial_unpad	spatial_unpad	spatial_unpad
	Max Seq Length	4,096	4,096	8,192	8,192
	A100 GPUs	2×8	2×8	2×8	2×8

Table 5. Training schedule across four curriculum stages.

selected vision layer is -2 . Each stage is trained for one epoch with per-device batch sizes of $\{8, 4, 2, 2\}$ on a 2×8 A100 GPU setup.

Overall, this four-stage training pipeline starts from general visual perception (Stages 1–2), advances to multi-view processing (Stage 3), and culminates in domain-specific EM expertise (Stage 4). The combination of curriculum design, dataset mixing, and decoupled optimization balances stability and plasticity, leading to robust end-to-end EM perception, category-level recognition, and downstream decision making, while keeping the total compute and sequence lengths within the limits reported in Table 5.

B. Details of Evaluation Metrics

To evaluate free-form answers in the `OpenQA#` setting, we adopt four standard automatic metrics. BLEU-4 (BLEU4) measures local n-gram precision (1–4 grams) with a brevity penalty [48]. ROUGE is recall oriented, including ROUGE-N and ROUGE-L to assess coverage via n-gram recall and LCS-based F-score, respectively [49]. METEOR performs alignment-based matching, combines precision and recall with a fragmentation penalty, and allows stem and synonym matches to capture semantic paraphrases [50]. CIDEr employs TF-IDF-weighted n-gram representations and

cosine similarity against multiple references to emphasize consensus with the reference set [51].

C. Complementary Experiments

C.1. Ablation Study on Domain-Specific EM Expertise Stage (Stage-4)

To investigate the impact of our curriculum learning strategy, we conduct a crucial ablation study focusing on the data composition of the domain-specific EM expertise stage. We compare two models: 1) **PReD⁻**, which is fine-tuned in Stage 4 *exclusively* on our specialized **PReD-1.3M** dataset. 2) **PReD**, which is fine-tuned on a *mixture* of the PReD-1.3M dataset and the general visual corpora from the first three stages.

We evaluate both models on two fronts: their performance on specialized domain tasks and their general multimodal capabilities.

Performance on Domain-Specific EM Tasks.

Our evaluation on specialized EM tasks uses two types of metrics. For the five recognition and reasoning tasks (SSD, SPE, MR, PR, EI), we report standard **accuracy**. For the text-generation task, AJSD, we calculate a composite score from four standard metrics: BLEU-4, ROUGE-L, METEOR, and CIDEr. To ensure a consistent scale for averaging across all tasks,

Method	SSD	SPE	MR	PR	EI	AJSD	Average
PReD⁻ (w/o General Corpora)	83.55	86.37	72.40	74.40	71.83	50.05	73.10
PReD (Ours)	83.40	85.70	72.00	72.00	69.43	48.59	71.85

Table 6. **Performance comparison on the specialized EM benchmark.** The variant fine-tuned exclusively on EM data (**PReD⁻**) achieves a marginal performance gain on these domain-specific tasks. As shown in Table 7, this slight advantage comes at the cost of a severe degradation in general multimodal capabilities.

Method	MMStar	AI2D	HallusionBench	SEEDBench IMG	POPE	ScienceQA TEST	Average
PReD ⁻ (w/o General Corpora)	39.47	54.44	8.10	56.75	0.74	56.02	35.92
PReD (Ours)	50.20	74.32	54.47	73.67	70.37	69.16	65.37

Table 7. **Ablation study on mixing general-domain data in the final training stage.** We compare our full model (**PReD**) against a variant (**PReD⁻**) that was fine-tuned exclusively on the specialized EM dataset without the general visual corpora. Mixing general-domain data significantly prevents catastrophic forgetting and boosts performance across general benchmarks.

this composite score is derived by averaging the four metrics and multiplying the result by 100.

The detailed performance comparison is presented in Table 6. The hyper-specialized **PReD⁻** model, trained without general corpora, achieves a slightly higher average score of 73.10% compared to our final **PReD** model’s 71.85%. This indicates that while focusing solely on domain data yields a marginal performance gain on specialized tasks, it comes with a significant trade-off.

Performance on General Multimodal Benchmarks. The nature of this trade-off becomes clear when evaluating general capabilities, as presented in Table 7. Here, the benefit of our data mixing strategy is dramatic. Our full model, **PReD**, achieves a strong average score of 65.37%. In stark contrast, the performance of **PReD⁻** collapses to 35.92%. This significant gap highlights that fine-tuning exclusively on specialized data leads to severe **catastrophic forgetting** of general multimodal knowledge acquired in earlier stages.

In summary, these results demonstrate the critical role of mixing general-domain data in the final training stage. While a narrow focus on EM data yields a slight edge (+1.25%) in specialized accuracy, it catastrophically degrades general abilities. Our strategy successfully mitigates this issue, creating a robust model that excels in its specific domain without sacrificing its foundational multimodal competence. This balance is crucial for developing a true EM foundation model.

C.2. Ablation Study on Input Modalities

To understand the contribution of each input modality, we conducted a comprehensive ablation study across two distinct tasks: modulation recognition (a clas-

sification task, Table 8) and anti-jamming decision-making (a generation task, Table 9). For all experiments, unselected modalities were replaced with zero-filled placeholders to maintain consistent input dimensionality. Our findings reveal consistent patterns across both tasks.

Finding 1: IQ as the Foundational Modality.

Across both tasks, the **IQ** modality consistently proves to be the most informative when used alone. It achieves the highest single-modality accuracy in modulation recognition (50.8%) and dominates all metrics in anti-jamming decision-making (0.363 average score). This is physically expected, as IQ data represents the lossless, raw complex-valued information of the signal containing all amplitude and phase variations. It carries the strongest discriminative cues, forming a robust foundation for downstream tasks.

Finding 2: Complementarity vs. Redundancy.

The combination of modalities highlights clear synergistic and redundant relationships. For instance, in modulation recognition, *Constellation+IQ* (64.2%) significantly outperforms the sum of its parts. This demonstrates that while IQ provides temporal details, the Constellation diagram explicitly visualizes the modulation state space (symbol grid), transforming statistical distributions into distinct geometric visual patterns that are easier for the vision encoder to capture. Conversely, *FFT+STFT* (37.8%) performs poorly, indicating substantial redundancy. Since STFT already encapsulates spectral information over time, the global spectral statistics provided by FFT offer limited additional entropy compared to the time-frequency view. This pattern holds in the decision-making task, where combinations including both IQ

Constellation	FFT	STFT	IQ	Accuracy
✓	×	×	×	43.4
×	✓	×	×	35.0
×	×	✓	×	30.2
×	×	×	✓	50.8
✓	✓	×	×	54.8
✓	×	✓	×	58.4
✓	×	×	✓	64.2
×	✓	✓	×	37.8
×	✓	×	✓	55.6
×	×	✓	✓	57.0
✓	✓	✓	×	59.2
✓	✓	×	✓	68.8
✓	×	✓	✓	70.0
×	✓	✓	✓	61.0
✓	✓	✓	✓	72.0

Table 8. MR accuracy (%) for different modality combinations. The optimal result is highlighted in bold.

and other modalities like *STFT* or *Constellation* yield top results within their cardinality groups.

Finding 3: The Efficiency-Accuracy Sweet Spot. While using all four modalities consistently yields the best performance on both tasks (72.0% and 0.4860), a clear point of diminishing returns emerges. The three-modality combination of *Constellation+STFT+IQ* achieves 70.0% accuracy in recognition and an average score of 0.414 in decision-making. These results represent 97.2% and 85.1% of the full four-modality performance, respectively. This makes the *Constellation+STFT+IQ* combination a highly effective trade-off. It successfully covers the three critical physical dimensions of EM signals: temporal dynamics (IQ), spectral footprint (STFT), and modulation topology (Constellation), rendering the marginal gain from adding the final FFT modality relatively small.

In summary, our cross-task ablation provides clear guidance for modality selection. **IQ** is indispensable as the information source. **Constellation** and **STFT** provide critical, complementary perspectives that explicitly visualize features hidden in the time domain. **FFT**, while beneficial, often overlaps with STFT and offers the least unique information. For resource-constrained applications, the *Constellation+STFT+IQ* trio is an optimal choice, while the full four-modality input should be used when maximizing performance is the primary goal.

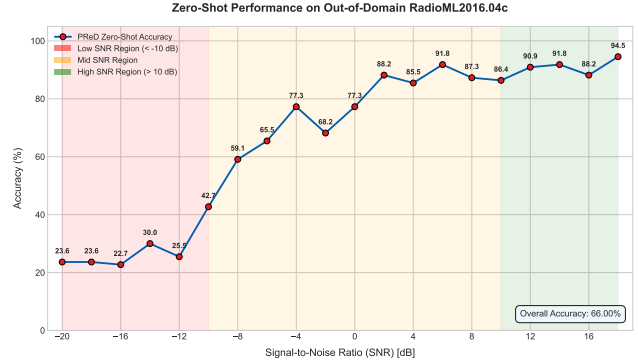


Figure 6. Zero-shot modulation recognition accuracy of PReD on the OOD RadioML2016.04c dataset across SNR levels. The overall accuracy is 66.0%.

C.3. Out-of-Domain Generalization for Modulation Recognition

To further assess the generalization capabilities of PReD beyond its training distribution, we conducted a challenging out-of-domain (OOD) evaluation. While PReD was trained for modulation recognition using only the ‘RadioML2016.10a’ dataset, we evaluated its zero-shot performance on the unseen ‘RadioML2016.04c’ dataset, which features different channel conditions and signal characteristics. We constructed a multiple-choice question benchmark by sampling 10 signals for each modulation type at every available Signal-to-Noise Ratio (SNR), resulting in a total of 2,200 evaluation samples.

On this challenging OOD benchmark, PReD achieved a strong overall accuracy of **66.0%** (1452/2200), demonstrating robust generalization to unseen signal environments without any fine-tuning. To gain deeper insights into the model’s robustness to noise, we analyzed its performance across different SNR levels, as detailed in Figure 6. The results reveal a clear and physically expected trend: performance is modest in the **low-SNR regime** (< -10 dB) where signals are heavily corrupted by noise; it then **improves dramatically in the mid-SNR range** (-10 dB to 10 dB), and finally **stabilizes at a high level in the high-SNR range** (> 10 dB).

This behavior, which mirrors the performance curves of specialized recognition models, confirms that PReD has learned to extract meaningful physical features from the signals rather than merely overfitting to the source dataset. This validates its potential as a robust foundation model for electromagnetic signal processing.

Input Modality	BLEU4	ROUGE	METEOR	CIDEr	Average
<i>Constellation</i>	0.069	0.329	0.227	0.405	0.258
<i>FFT</i>	0.056	0.305	0.194	0.381	0.234
<i>STFT</i>	0.094	0.374	0.267	0.447	0.2955
<i>IQ</i>	0.149	0.438	0.337	0.530	0.363
<i>Constellation+FFT</i>	0.070	0.331	0.227	0.409	0.259
<i>Constellation+STFT</i>	0.104	0.384	0.279	0.465	0.308
<i>Constellation+IQ</i>	0.168	0.464	0.359	0.549	0.385
<i>FFT+STFT</i>	0.095	0.373	0.267	0.449	0.296
<i>FFT+IQ</i>	0.153	0.441	0.341	0.534	0.367
<i>STFT+IQ</i>	0.185	0.488	0.381	0.567	0.405
<i>Constellation+FFT+STFT</i>	0.102	0.379	0.276	0.464	0.305
<i>Constellation+FFT+IQ</i>	0.168	0.463	0.357	0.548	0.384
<i>Constellation+STFT+IQ</i>	0.193	0.499	0.388	0.575	0.414
<i>FFT+STFT+IQ</i>	0.185	0.489	0.381	0.567	0.405
<i>Constellation+FFT+STFT+IQ</i>	0.253	0.559	0.515	0.617	0.486

Table 9. Ablation on input modalities for the anti-jamming strategy decision-making task.

C.4. Performance Analysis under Varying SNR

To provide a more granular view of PReD’s robustness, we analyze the performance of the **EM Recognition** tasks under varying SNRs. Within this category, we present the results for **MR** and **PR**, as their underlying benchmarks contain explicit SNR labels suitable for this analysis. The **EI** task is excluded from this analysis because its dataset consists of real-world captured signals that lack ground-truth SNR annotations.

As illustrated in Figure 7, both tasks exhibit a remarkably consistent and physically expected trend: model accuracy degrades gracefully as the SNR decreases. This demonstrates that PReD has learned to leverage signal quality in a meaningful way, reinforcing its capability as a robust foundation model for the EM domain. The performance drop is most pronounced in the negative SNR regime, where the signal power is weaker than the noise power, yet the model retains non-trivial recognition capabilities.

D. Visual Analysis of PReD-Bench and Benchmark Results

This section offers a deeper, more intuitive understanding of our benchmark and results through both visual analysis and qualitative examples. First, we present two complementary visualizations: a hierarchical chart to break down the composition of PReD-Bench and a radar chart to summarize the comparative model performances discussed in the main text. Following this quantitative overview, we provide a series of rep-

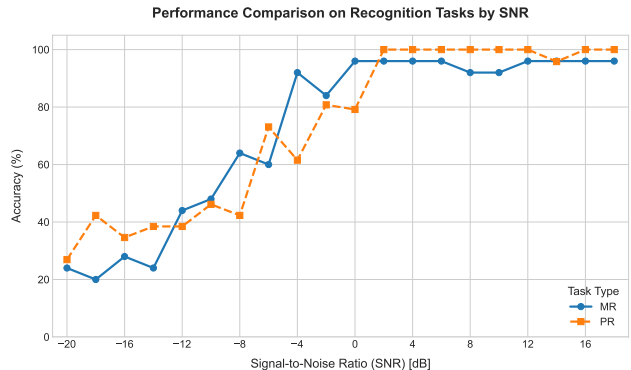


Figure 7. Performance comparison on **MR** and **PR** task across varying SNR levels. Both tasks show a similar graceful degradation, highlighting the model’s consistent and robust behavior against noise.

representative qualitative examples to concretely illustrate PReD’s capabilities across the full range of EM tasks.

D.1. Hierarchical Composition of PReD-Bench

Figure 8 offers a hierarchical visualization of the PReD-Bench’s composition. The chart is structured into three concentric rings representing different levels of granularity:

- **Innermost Ring (Dimensions):** This ring shows the three core capabilities evaluated by the benchmark: **Perception** (59.1%), **Recognition** (17.2%), and **Decision-Making** (23.6%).
- **Middle Ring (Tasks):** This ring breaks down

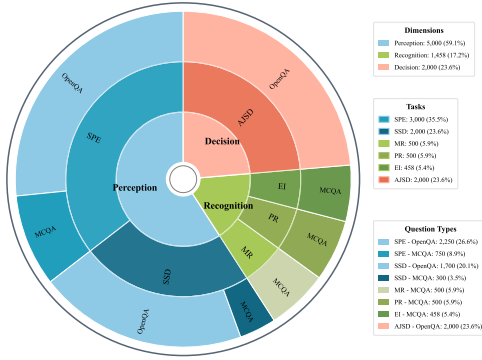


Figure 8. Hierarchical composition of the PRoD-Bench, showing the distribution across three core dimensions, six specific tasks, and two primary question types (OpenQA and MCQA).

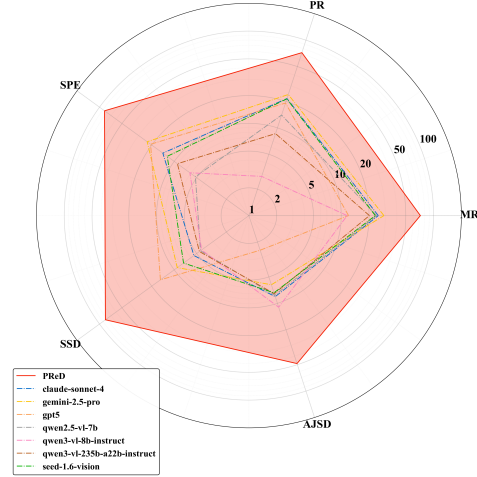


Figure 9. Log-scale radar plot of averaged performance over five EM tasks. PRoD demonstrates superior performance across all evaluated tasks.

the dimensions into six specific tasks. It details the sample distribution among SPE (35.5%), SSD (23.6%), MR (5.9%), PR (5.9%), EI (5.4%), and AJSD (23.6%).

- Outermost Ring (Question Types):** The final ring specifies the question format for each task. It shows that Perception tasks (SPE, SSD) are designed with a mix of **OpenQA** and **MCQA** formats, while the majority of Recognition tasks (MR, PR, EI) are exclusively **MCQA**. The Decision-Making task (AJSD) is designed as a pure **OpenQA** generative task.

This layered structure illustrates the benchmark’s comprehensive design, ensuring a balanced evaluation across diverse EM tasks and reasoning formats.

D.2. Comparative Performance Visualization on EM Tasks

The log-scale radar chart in Fig. 9 summarizes the cross-task average performance across five representative EM tasks. **PRoD consistently forms the outer envelope and yields the largest enclosed area**, highlighting its dominant advantage throughout the full EM pipeline.

In contrast, **general-purpose MLLMs exhibit a clear performance gap between foundational and advanced tasks**. They maintain moderate capabilities on foundational tasks involving **perception (SPE/SSD)** and **recognition (MR/PR)**. However, their performance collapses on the advanced, open-ended generative task of **decision-making (AJSD)**. This is particularly evident for models like GPT-5, Gemini-2.5-Pro, and Claude-Sonnet-4, all of which show a severe contraction toward the AJSD axis.

This collective pattern aligns with the tabulated

results and demonstrates the critical limitation of general-purpose MLLMs when transitioning from pattern recognition to applied, open-ended reasoning. This further validates the effectiveness of our domain-specific modeling and multi-stage curriculum in building true end-to-end intelligence.

D.3. Qualitative Examples on PRoD-Bench Tasks

To provide a qualitative illustration of PRoD’s capabilities, we present representative examples for each of the six core tasks defined in the PRoD-Bench. These examples, shown in Figure 10, showcase the model’s ability to handle a diverse range of inputs and generate accurate, context-aware responses across the full spectrum of EM intelligence: from foundational perception and recognition to complex decision-making. It is worth noting that for the open-ended nature of Modulation Recognition, Protocol Recognition, and Emitter Identification tasks, where different expressions can convey the same meaning, we standardized the evaluation in our test set by removing the open-ended response format for these specific tasks to ensure consistent and objective assessment.

Each subfigure presents a user query, which may include single or multiple signal images, followed by the detailed, human-like response generated by PRoD. These examples complement the quantitative results in the main paper by offering a direct view into the model’s reasoning and generative abilities.

OpenQA*

Please analyze this time-domain amplitude plot. First, determine if a signal exists. You must answer yes or no and wrap the answer with `<exist>` and `</exist>`. If `<exist>yes</exist>`, specify the start time using `<start>` and the end time using `<end>`... (in microseconds)

`<exist>yes</exist>`. Time range: from `<start>2.6</start>` to `<end>21.8</end>` microseconds.

MCQA

Please review the signal diagram and choose the option that best corresponds to the signal's time boundaries. Wrap your answer with `<answer>` and `</answer>`.

`<answer>A</answer>`

A. Signal present with start: 2.6±1, end: 21.8±1 microseconds
 B. Signal present with start: 19.7±1, end: 30.8±1 microseconds
 C. No signal is present in the plot
 D. Signal present with start: 11.7±1, end: 32.7±1 microseconds
 E. Unable to answer

(a) Task 1: Signal Segment Detection (SSD)

OpenQA*

Can the basic signal parameters be determined from this time-domain plot? List `td`, `pw`, `pri`, and `np` using `<td>`, `<pw>`, `<pri>`, `<np>` tags without any additional content.

Signal parameters: Time delay `<td>6.3</td>`us, pulse width `<pw>10.7</pw>`us, repetition interval `<pri>20.0</pri>`us, pulse count `<np>4</np>`.

MCQA

Looking at this waveform, can you help me read the pulse repetition interval? Choose the correct option from the choices below. Only answer with ABCDE options, and wrap your answer in `<answer>` tags without explanations.

`<answer>A</answer>`

A. 20.1±1 us
 B. 26.5±1 us
 C. 11.2±1 us
 D. 63.6±1 us
 E. Unable to answer

(b) Task 2: Signal Parameter Estimation (SPE)

OpenQA*

Please determine the modulation type of the signal based on the following four images (IQ constellation diagram, FFT spectrum diagram, STFT time-frequency diagram, and IQ component diagram). Output only the final result, and place it within `<mode>`...`</mode>`.

`<mode>QAM16</mode>`

MCQA

Determine the modulation type of the signal from the following four images (IQ constellation diagram, FFT spectrum diagram, STFT time-frequency diagram, and IQ component diagram). Which of the following is correct?

A. GFSK
 B. CFSK
 C. QAM16
 D. WBFM
 E. unable to answer
 Please answer only with the letter corresponding to the correct answer, in the format: `<answer>`...`</answer>`.

`<answer>C</answer>`

(c) Task 3: Modulation Recognition (MR)

OpenQA*

Please observe the provided IQ constellation diagram, FFT spectrum diagram, STFT time-frequency diagram, and IQ component diagram. Based on these images, identify the protocol type used. Output only the protocol result in the format: `<protocol>`...`</protocol>`.

`<protocol>SHORT-RANGE</protocol>`

MCQA

Determine the protocol type of the signal from the following four images (IQ constellation diagram, FFT spectrum diagram, STFT time-frequency diagram, and IQ component diagram). Which of the following is correct?

A. AIRBORNE-DETECTION
 B. AM RADIO
 C. SHORT-RANGE
 D. GROUND MAPPING
 E. Unable to answer
 Please answer only with the letter corresponding to the correct answer, in the format: `<answer>`...`</answer>`.

`<answer>C</answer>`

(d) Task 4: Protocol Recognition (PR)

OpenQA*

These signal diagrams come from one emitter. Please identify which emitter it is. Output format: `<emitter>`...`</emitter>`.

`<emitter>USRP_X310_15</emitter>`

MCQA

Based on the four signal images (IQ constellation, FFT spectrum, STFT spectrogram, and IQ components), which of the following emitters transmitted this signal?

A. USRP_X310_4
 B. USRP_X310_15
 C. USRP_X310_1
 D. USRP_X310_14
 E. Unable to answer
 Please answer only with the letter corresponding to the correct answer, in the format: `<answer>`...`</answer>`.

`<answer>B</answer>`

(e) Task 5: Emitter Identification (EI)

OpenQA#

Analyze the signal plots provided. What countermeasures should be implemented to ensure reliable communication in the presence of this interference?

Jamming_type is : Widecomb
 Interference Resistance Strategies:
 - Time Domain Interference Resistance Strategy: Implement randomized burst sending schemes to disrupt interference synchronization,

(f) Task 6: Anti-Jamming Strategy Decision-making (AJSD)

Figure 10. Qualitative examples of PRoD's performance across the six core tasks of PRoD-Bench. Each panel showcases a different capability, from perception (a, b), to recognition (c, d, e), and finally to complex decision-making (f).

References

- [1] Haotian Liu, Chunyuan Li, Qingyang Wu, and Yong Jae Lee. Visual instruction tuning. volume 36, pages 34892–34916, 2023. 2, 3
- [2] Junnan Li, Dongxu Li, Silvio Savarese, and Steven Hoi. Blip-2: Bootstrapping language-image pre-training with frozen image encoders and large language models. volume 202, pages 19730–19742, 2023. 2, 3
- [3] OpenAI. Gpt-4v(ision) system card, 2023. System Card. 2, 8
- [4] Rohit Girdhar, Alaaeldin El-Nouby, Zhuang Liu, Man- nat Singh, Kalyan Vasudev Alwala, Armand Joulin, and Ishan Misra. Imagebind: One embedding space to bind them all. In *CVPR*, pages 15180–15190, 2023. 2, 3
- [5] Jiawei Shao, Jingwen Tong, Qiong Wu, Wei Guo, Zi- jian Li, Zehong Lin, and Jun Zhang. Wirelessllm: Em- powering large language models towards wireless intel- ligence. *arXiv preprint arXiv:2405.17053*, 2024. 2, 3
- [6] Shuai Chen, Yong Zu, Zhixi Feng, Shuyuan Yang, Mengchang Li, Yue Ma, Jun Liu, Qiukai Pan, Xin- lei Zhang, and Changjun Sun. Radiollm: Introducing large language model into cognitive radio via hybrid prompt and token reprogrammings. *arXiv preprint arXiv:2501.17888*, 2025. 2, 3
- [7] Haolin Zheng, Ning Gao, Donghong Cai, Shi Jin, and Michail Matthaiou. Uav individual identification via distilled rf fingerprints-based llm in isac networks. *IEEE Wireless Communications Letters*, pages 1–1, 2025. 2, 3
- [8] Hongye Quan, Wanli Ni, Tong Zhang, Xiangyu Ye, Ziyi Xie, Shuai Wang, Yuanwei Liu, and Hui Song. Large language model agents for radio map genera- tion and wireless network planning. *IEEE Netw. Lett.*, 7(3):166–170, 2025. 2
- [9] Chenxu Wang, Xumiao Zhang, Runwei Lu, Xian- shang Lin, Xuan Zeng, Xinlei Zhang, Zhe An, Gong- wei Wu, Jiaqi Gao, Chen Tian, Guihai Chen, Guyue Liu, Yuhong Liao, Tao Lin, Dennis Cai, and En- nan Zhai. Towards llm-based failure localization in production-scale networks. In *Proceedings of the ACM SIGCOMM 2025 Conference, SIGCOMM 2025, São Francisco Convent, Coimbra, Portugal, September 8- 11, 2025*, pages 496–511, 2025. 2
- [10] Uma Maheswari Natarajan, Raghuram Bharadwaj Diddigi, and Jyotsna Bapat. Rag-inspired intent-based solution for intelligent autonomous networks. In *17th International Conference on COMMunication Systems and NETWORKS, COMSNETS 2025, Bengaluru, India, January 6-10, 2025*, pages 413–421. IEEE, 2025. 2
- [11] Ziheng Qin, Yuheng Ji, Renshuai Tao, Yuxuan Tian, Yuyang Liu, Yipu Wang, and Xiaolong Zheng. Scaling up ai-generated image detection via generator-aware prototypes. *arXiv preprint arXiv:2512.12982*, 2025. 2
- [12] Timothy J. O’Shea, Johnathan Corgan, and T. Charles Clancy. Convolutional radio modulation recognition networks. pages 213–226, 2016. 2
- [13] Timothy James O’Shea, Tamoghna Roy, and T. Charles Clancy. Over-the-air deep learning based radio signal classification. *IEEE Journal of Selected Topics in Signal Processing*, 12(1):168–179, 2018. 2
- [14] Kürşat Tekbyk, Ali Rıza Ekti, Ali Görçin, Güneş Karabulut Kurt, and Cihat Keçeci. Ro- bust and fast automatic modulation classification with cnn under multipath fading channels. pages 1–6, 2020. 2
- [15] Timothy J. O’Shea, Johnathan Corgan, and T. Charles Clancy. Unsupervised representation learning of struc- tured radio communication signals. pages 1–5, 2016. 2
- [16] Timothy J. O’Shea, Latha Pemula, Dhruv Batra, and T. Charles Clancy. Radio transformer networks: At- tention models for learning to synchronize in wireless systems. pages 662–666, 2016.
- [17] Timothy J. O’Shea, Seth Hitefield, and Johnathan Corgan. End-to-end radio traffic sequence recognition with recurrent neural networks. pages 277–281, 2016. 2
- [18] Yuheng Ji, Huajie Tan, Jiayu Shi, Xiaoshuai Hao, Yuan Zhang, Hengyuan Zhang, Pengwei Wang, Mengdi Zhao, Yao Mu, Pengju An, et al. Robobrain: A unified brain model for robotic manipulation from ab- stract to concrete. In *Proceedings of the Computer Vi- sion and Pattern Recognition Conference*, pages 1724– 1734, 2025. 3
- [19] Huajie Tan, Yuheng Ji, Xiaoshuai Hao, Xiansheng Chen, Pengwei Wang, Zhongyuan Wang, and Shang- hang Zhang. Reason-rft: Reinforcement fine-tuning for visual reasoning of vision language models. In *The Thirty-ninth Annual Conference on Neural Informa- tion Processing Systems*, 2025. 3
- [20] Deyao Zhu, Jun Chen, Xiaoqian Shen, Xiang Li, and Mohamed Elhoseiny. Minigpt-4: Enhancing vision- language understanding with advanced large language models. *arXiv preprint*, 2023. 3
- [21] Jinze Bai, Shuai Bai, Shusheng Yang, Shijie Wang, Sinan Tan, Peng Wang, Junyang Lin, Chang Zhou, and Jingren Zhou. Qwen-vl: A versatile vision- language model for understanding, localization, text reading, and beyond, 2023. 3
- [22] Jean-Baptiste Alayrac, Jeff Donahue, Pauline Luc, An- toine Miech, Iain Barr, Yana Hasson, Karel Lenc, A. Mensch, Katie Millican, Malcolm Reynolds, Roman Ring, Eliza Rutherford, Serkan Cabi, Tengda Han, Zhitao Gong, Sina Samangooei, Marianne Monteiro, Jacob Menick, Sebastian Borgeaud, Andy Brock, Aida Nematzadeh, Sahand Sharifzadeh, Mikolaj Binkowski, Ricardo Barreira, Oriol Vinyals, Andrew Zisserman, and Karen Simonyan. Flamingo: A visual language model for few-shot learning. *arXiv preprint*, 2022. 3
- [23] Zhiliang Peng, Wenhui Wang, Li Dong, Yaru Hao, Shaohan Huang, Shuming Ma, and Furu Wei. Kosmos- 2: Grounding multimodal large language models to the world. *arXiv preprint*, 2023. 3

- [24] Wenhao Wu, Huanjin Yao, Mengxi Zhang, Yuxin Song, Wanli Ouyang, and Jingdong Wang. Gpt4vis: What can gpt-4 do for zero-shot visual recognition? *arXiv preprint arXiv:2311.15732*, 2024. 3
- [25] Yipu Wang, Yuheng Ji, Yuyang Liu, Enshen Zhou, Ziqiang Yang, Yuxuan Tian, Ziheng Qin, Yue Liu, Huajie Tan, Cheng Chi, et al. Towards cross-view point correspondence in vision-language models. *arXiv preprint arXiv:2512.04686*, 2025. 3
- [26] Yuheng Ji, Yipu Wang, Yuyang Liu, Xiaoshuai Hao, Yue Liu, Yuting Zhao, Huaihai Lyu, and Xiaolong Zheng. Visualtrans: A benchmark for real-world visual transformation reasoning. *arXiv preprint arXiv:2508.04043*, 2025. 3
- [27] Nada Abdel Khalek, Deemah H. Tashman, and Walaa Hamouda. Advances in machine learning-driven cognitive radio for wireless networks: A survey. *IEEE Communications Surveys & Tutorials*, 26(2):1201–1237, 2024. 3
- [28] Hengtao He, Shi Jin, Chao-Kai Wen, Feifei Gao, Geoffrey Ye Li, and Zongben Xu. Model-driven deep learning for physical layer communications. *IEEE Wireless Communications*, 26(5):77–83, 2019. 3
- [29] Yuheng Ji, Huajie Tan, Cheng Chi, Yijie Xu, Yuting Zhao, Enshen Zhou, Huaihai Lyu, Pengwei Wang, Zhongyuan Wang, Shanghang Zhang, et al. Mathsticks: A benchmark for visual symbolic compositional reasoning with matchstick puzzles. *arXiv preprint arXiv:2510.00483*, 2025. 3
- [30] Yuheng Ji, Yue Liu, Zhicheng Zhang, Zhao Zhang, Yuting Zhao, Xiaoshuai Hao, Gang Zhou, Xingwei Zhang, and Xiaolong Zheng. Enhancing adversarial robustness of vision-language models through low-rank adaptation. In *Proceedings of the 2025 International Conference on Multimedia Retrieval*, pages 550–559, 2025. 3
- [31] Jason Wei, Maarten Bosma, Vincent Y. Zhao, Kelvin Guu, Adams Wei Yu, Brian Lester, Nan Du, Andrew M. Dai, and Quoc V. Le. Finetuned language models are zero-shot learners. In *The Tenth International Conference on Learning Representations, ICLR 2022, Virtual Event, April 25-29, 2022*. OpenReview.net, 2022. 4
- [32] Zixian Huang, Ao Wu, Jiaying Zhou, Yu Gu, Yue Zhao, and Gong Cheng. Clues before answers: Generation-enhanced multiple-choice QA. In *Proceedings of the 2022 Conference of the North American Chapter of the Association for Computational Linguistics: Human Language Technologies, NAACL 2022, Seattle, WA, United States, July 10-15, 2022*, pages 3272–3287. Association for Computational Linguistics, 2022. 4
- [33] Todor Mihaylov, Peter Clark, Tushar Khot, and Ashish Sabharwal. Can a suit of armor conduct electricity? A new dataset for open book question answering. In *Proceedings of the 2018 Conference on Empirical Methods in Natural Language Processing, Brussels, Belgium, October 31 - November 4, 2018*, pages 2381–2391. Association for Computational Linguistics, 2018. 5
- [34] Yuheng Ji, Yuyang Liu, Huajie Tan, Xuchuan Huang, Fanding Huang, Yijie Xu, Cheng Chi, Yuting Zhao, Huaihai Lyu, Peterson Co, et al. Prm-as-a-judge: A dense evaluation paradigm for fine-grained robotic auditing. *arXiv preprint arXiv:2603.21669*, 2026. 6
- [35] Haotian Liu, Chunyuan Li, Qingyang Wu, and Yong Jae Lee. Visual instruction tuning. In *Advances in Neural Information Processing Systems*, volume 36, pages 34892–34916, 2023. 6
- [36] Qwen Team. Qwen3 technical report, 2025. 6, 8
- [37] Alec Radford, Jong Wook Kim, Chris Hallacy, Aditya Ramesh, Gabriel Goh, Sandhini Agarwal, Girish Sastry, Amanda Askell, Pamela Mishkin, Jack Clark, Gretchen Krueger, and Ilya Sutskever. Learning transferable visual models from natural language supervision. In *Proceedings of the 38th International Conference on Machine Learning, ICML 2021, 18-24 July 2021, Virtual Event*, volume 139 of *Proceedings of Machine Learning Research*, pages 8748–8763. PMLR, 2021. 6
- [38] Qwen Team. Qwen2.5-vl, January 2025. 8
- [39] Seed Team. Seed1.5-vl technical report, 2025. 8
- [40] Anthropic. Claude-3.5, November 2024. Accessed: 2024-11-02. 8
- [41] OpenAI. Gpt-5, 2025. 8
- [42] G. Gemini team, 2025. 8
- [43] Jinze Bai, Shuai Bai, Shusheng Yang, Shijie Wang, Sinan Tan, Peng Wang, Junyang Lin, Chang Zhou, and Jingren Zhou. Qwen-vl: A versatile vision-language model for understanding, localization, text reading, and beyond. *arXiv preprint arXiv:2308.12966*, 2023. 8
- [44] Feng Li, Renrui Zhang, Hao Zhang, Yuanhan Zhang, Bo Li, Wei Li, Zejun Ma, and Chunyuan Li. Llava-next-interleave: Tackling multi-image, video, and 3d in large multimodal models, 2024. 8
- [45] Haoyu Lu, Wen Liu, Bo Zhang, Bingxuan Wang, Kai Dong, Bo Liu, Jingxiang Sun, Tongzheng Ren, Zhuoshu Li, Yaofeng Sun, Chengqi Deng, Hanwei Xu, Zhenda Xie, and Chong Ruan. Deepseek-vl: Towards real-world vision-language understanding, 2024. 8
- [46] Yuan Yao, Tianyu Yu, Ao Zhang, Chongyi Wang, Junbo Cui, Hongji Zhu, Tianchi Cai, Haoyu Li, Weilin Zhao, Zhihui He, et al. Minicpm-v: A gpt-4v level mllm on your phone. *arXiv preprint arXiv:2408.01800*, 2024. 8
- [47] Lin Chen, Jinsong Li, Xiaoyi Dong, Pan Zhang, Conghui He, Jiaqi Wang, Feng Zhao, and Dahua Lin. Sharegpt4v: Improving large multi-modal models with better captions, 2023. 8
- [48] Kishore Papineni, Salim Roukos, Todd Ward, and Wei-Jing Zhu. Bleu: a method for automatic evaluation of machine translation. In *Proceedings of the 40th Annual*

Meeting of the Association for Computational Linguistics, pages 311–318, Philadelphia, USA, 2002. Association for Computational Linguistics. [10](#)

- [49] Chin-Yew Lin. Rouge: A package for automatic evaluation of summaries. In *Text Summarization Branches Out*, pages 74–81, Barcelona, Spain, 2004. Association for Computational Linguistics. [10](#)
- [50] Satanjeev Banerjee and Alon Lavie. Meteor: An automatic metric for MT evaluation with improved correlation with human judgments. In *Proceedings of the ACL Workshop on Intrinsic and Extrinsic Evaluation Measures for Machine Translation and/or Summarization*, pages 65–72, Ann Arbor, USA, 2005. Association for Computational Linguistics. [10](#)
- [51] Ramakrishna Vedantam, C. Lawrence Zitnick, and Devi Parikh. CIDEr: Consensus-based image description evaluation. In *Proceedings of the IEEE Conference on Computer Vision and Pattern Recognition*, pages 4566–4575, Boston, USA, 2015. IEEE. [10](#)